

# Structural Characterization of Langmuir–Blodgett Films Derived from Multisulfur Heterocycles

Y. Zhang, M. A. Firestone, T. B. Rauchfuss,\* and P. W. Bohn\*

Department of Chemistry, Beckman Institute, and Materials Research Laboratory, University of Illinois at Urbana–Champaign, 600 S. Mathews Street, Urbana, Illinois 61801

Received: April 17, 1996<sup>⊗</sup>

A novel multisulfur heterocyclic compound with alkyl chains,  $C_3S_5(C_{18}H_{37})_2$  (4,5-bis(octadecylthio)-1,3-dithiole-2-thione), has been synthesized and fabricated into Langmuir–Blodgett (LB) films. The structure of this film on  $SiO_2$  slides has been studied using X-ray photoelectron spectroscopy (XPS) and IR and UV transmission linear dichroism (LD) measurements. From the isotherm, it is known that the Langmuir film at the air–water interface is a bilayer. Angle-resolved XPS of films transferred to  $SiO_2$  show that the alkyl chains of the molecule form the topmost layer of the film, with the  $C_3S_5$  ring underneath the alkyl layer. Electronic structure calculations indicate that the transition moment associated with the observed UV band lies coincident with the  $C_2$  axis of the  $C_3S_5$  ring group. In order to properly interpret the polarized absorption data, a simple model addressing the local field effect in LD measurements was developed. Incorporating measured information on the polarizability of the chromophore, UV and IR LD measurements showed the ring plane and the chains to be stacked at  $69^\circ$  and  $20^\circ$ , respectively, relative to the surface normal. These data coupled with the XPS results permitted a structural model to be constructed which accounts for the multilayer structure of the transferred film.

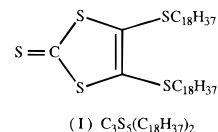
## I. Introduction

In recent years, with the development of the self-assembly (SA) and Langmuir–Blodgett (LB) techniques, organic molecules with unique properties have been incorporated into thin solid films with ordered structures.<sup>1,2</sup> Research in this area is motivated by a number of possible applications, e.g., the fabrication of nanometer scale molecular electronic devices. Among film-forming organic molecules, sulfur-containing compounds have received special interest, because the large van der Waals radius of sulfur promotes intermolecular electronic interactions. In addition to the vast literature on organic thiols,<sup>3</sup> multisulfur heterocycle compounds have long been of interest,<sup>4</sup> beginning with the discovery of low-dimensional electronic conductors containing tetrathiafulvalene (TTF).<sup>5</sup> Interest in this area of chemistry led to the development of a new generation of sulfur heterocycles derived from the reduction of carbon disulfide.<sup>6</sup> Of particular importance is the anion  $C_3S_5^{2-}$ , the isolation of which was greatly simplified by Hoyer and co-workers.<sup>7</sup> The significance of  $C_3S_5^{2-}$  is twofold: first, it can be easily functionalized through alkylation reactions, and second, the resulting dialkylated heterocycles can be converted into TTF analogs and related molecular electronic materials. Transition metals coordinated by  $C_3S_5^{2-}$  ligands have been shown to exhibit metal-like electronic or magnetic properties.<sup>8</sup>

The novel electronic properties in these multisulfur heterocycles make them an ideal subject for thin solid film research. Indeed, it has been reported that unsaturated carbon–sulfur ring compounds such as TTF derivatives and  $M(C_3S_5)_2^{2-}$  ( $M = Au, Cu, Zn$ , etc.) have been incorporated into LB films, although they require fatty acids to enhance their mechanical properties. These films become highly conducting upon oxidation.<sup>9</sup>

Structures of LB films containing multisulfur heterocycles have not been reported to date. In this study, a new compound,

$C_3S_5(C_{18}H_{37})_2$  (4,5-bis(octadecylthio)-1,3-dithiole-2-thione, **I**),



has been synthesized and its LB film-forming properties studied. The structure of this molecule as an adlayer on fused quartz has been investigated by transmission linear dichroism (LD), surface infrared spectroscopy, and X-ray photoelectron spectroscopy (XPS). Understanding of the electronic structure and interpretation of the LD results has been aided by the Hückel MO<sup>10</sup> and the semiempirical Pariser–Parr–Pople (PPP) calculations.<sup>11</sup> Proper interpretation of data from these different structural probes requires that the strongly interacting nature of the  $C_3S_5$  moieties be taken into account, particularly in the LD measurements. Thus, a subtheme of these investigations involves proper accounting for the local fields in the film during LD measurements. By considering the film as a dielectric medium and taking the local field effect into account properly, the effective refractive index of the film and consequently the orientation angle of a dipole can be obtained, thus enabling a detailed structural model for these  $C_3S_5$ -containing films to be constructed.

## II. Experimental Section

**2.1. Synthesis of  $C_3S_5(C_{18}H_{37})_2$  (I).** Samples of  $C_3S_5(C_{18}H_{37})_2$  were synthesized by the reaction of  $(Bu_4N)_2[Zn(C_3S_5)_2]$  with  $C_{18}H_{37}Br$  in tetrahydrofuran. After the insoluble solids were removed, the compound precipitated from the resulting solution while stored in a freezer overnight. The yield was 31.5%. It can also be isolated through other routes, such as alkaline cleavage of  $C_3S_5(COPh)_2$  and subsequent reaction with  $C_{18}H_{37}Br$ .  $(Bu_4N)_2[Zn(C_3S_5)_2]$  was synthesized previously.<sup>12</sup>  $C_{18}H_{37}Br$  and the solvents were purchased from Aldrich and used without further purification. The product is obtained

\* Authors to whom correspondence should be addressed.

<sup>⊗</sup> Abstract published in *Advance ACS Abstracts*, July 15, 1996.

as golden-yellow, air-stable crystalline needles and has been fully characterized by elemental analysis, FD-MS, UV-vis, FTIR, and  $^1\text{H-NMR}$  spectroscopies.

**2.2. LB Film Preparation.** All the LB film samples were prepared on a KSV 5000 trough. A 1 mM solution of **I** was prepared in  $\text{CHCl}_3$  (Baxter) and spread onto a deionized (DI) water subphase (Millipore, Model Milli-Q UV plus,  $\rho = 18.2 \text{ M}\Omega\text{-cm}$ ). The substrate had been pretreated by dipping three times in concentrated sulfuric acid at  $150^\circ\text{C}$  and rinsing in DI water, followed by immersion in 4:1 (v/v)  $\text{NH}_4\text{OH}/\text{H}_2\text{O}_2$ , rinsing, and drying under flowing  $\text{N}_2$ . The initial spreading density on the Langmuir trough was kept above  $54 \text{ \AA}^2/\text{molecule}$ . The  $\text{CHCl}_3$  was allowed to evaporate for 10 min before compression. The compression rates were typically 10 mm/min, limited by a maximum surface pressure change of 1 mN/(m $\cdot$ min). The film was stable at surface pressures  $\pi \leq 38 \text{ mN/m}$ . Films were transferred to  $25 \times 50 \times 1 \text{ mm}$  fused quartz slides (Quartz Scientific) at  $\pi = 20 \text{ mN/m}$  with a dipping rate of 15 mm/min. Under these conditions typical transfer ratios ( $\tau$ ) were  $2.10 \pm 0.05$ . However, the transfer ratio was found to depend strongly on the transfer conditions with values  $1.4 \leq \tau \leq 3.5$  being obtainable. The temperature was maintained at  $18 \pm 1^\circ\text{C}$  for all trough work.

**2.3. UV and IR Measurements.** UV measurements were carried out using a computer interfaced double-beam spectrometer (Varian, Cary-3). The spectra were recorded from 300 to 500 nm with a spectrometer resolution of 3 nm and a data interval of 1.5 nm. Fifty scans were averaged for each spectrum in order to achieve an adequate signal-to-noise ratio (peak-to-peak noise =  $2 \times 10^{-4}$  absorbance unit). The data acquisition time for each spectrum was 4 min. In LD measurements, a Glan-Taylor polarization prism (Melles-Griot) was used to obtain s- and p-polarized radiation.

Infrared spectra were obtained with a Bio-Rad FTS-60A spectrometer controlled by a Bio-Rad SPC 3200 data station. A  $\text{Hg}_x\text{Cd}_{1-x}\text{Te}$  detector was used. Each spectrum was collected from 2700 to  $3100 \text{ cm}^{-1}$  by averaging 256 scans with a resolution of  $4 \text{ cm}^{-1}$ . The polarizer used was ZnSe (NSG Precision Cell) with a useful wavelength range of 500–20 000  $\text{cm}^{-1}$ .

In the LD measurements, the sample was placed at the beam waist of the incident radiation with the film facing the radiation. The angle of incidence was measured against the surface normal and varied from  $0^\circ$  to  $80^\circ$  (for IR) or  $84^\circ$  (for UV-vis). Maximum angles near grazing incidence were limited by the divergences of the respective beams.

**2.4. X-ray Photoelectron Spectroscopy Measurements.** XPS spectra were obtained from a Perkin-Elmer ESCA system (PHI-5400). The excitation source was Mg  $K\alpha$  radiation (1253.6 eV). Photoelectrons were collected by a hemispherical analyzer. (Pass energy was 178.95 and 35.75 eV for survey and multiplex measurements, respectively.) Each spectrum was obtained by averaging several scans at a data interval of 0.05 eV. The acquisition time for each data point in a single scan was 0.1 s. In the angle-resolved measurements, the sample surface was rotated to obtain collection angles of  $0^\circ$  and  $75^\circ$  with respect to the surface normal. The samples were prepared immediately prior to XPS measurements.

**2.5. Molecular Electronic Structure Calculation.** Both the HMO and the PPP methods were used to calculate the electronic structure of the  $\text{C}_3\text{S}_5$  ring. The PPP MO calculation was carried out with limited configuration interaction (CI) treatment, using bond lengths and angles determined by X-ray crystallographic analysis of the  $\text{C}_3\text{S}_5$  ring.<sup>13</sup> The two-center repulsion integrals were computed by the Mataga-Nishimoto

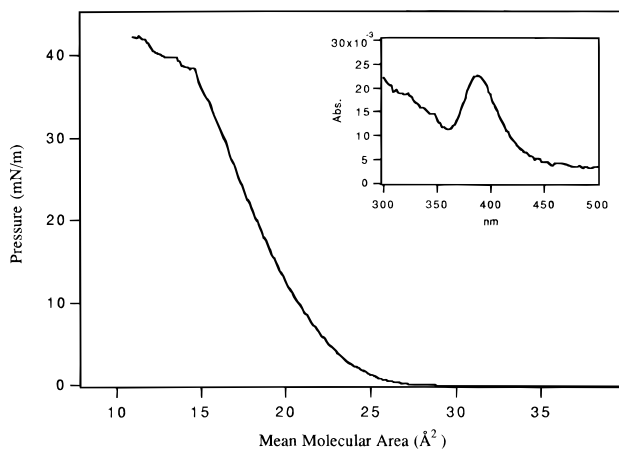


**Figure 1.** Langmuir isotherm of  $\text{C}_3\text{S}_5(\text{C}_{18}\text{H}_{37})_2$ . The linear portion of the isotherm yields an extrapolated mean molecular area,  $A = 22.4 \pm 0.2 \text{ \AA}^2$ . The inset shows the electronic absorption spectrum of the LB film of  $\text{C}_3\text{S}_5(\text{C}_{18}\text{H}_{37})_2$  on  $\text{SiO}_2$ .

method.<sup>14</sup> Carbon and sulfur parametrization was selected according to literature descriptions.<sup>15</sup> Parameters used in the HMO calculation were the same as IP and  $\beta_{xy}$  parameters in the PPP calculation.

### III. Results and Discussion

**3.1. Film Formation.** The pressure–area ( $\pi$ – $A$ ) isotherm of  $\text{C}_3\text{S}_5(\text{C}_{18}\text{H}_{37})_2$ , **I** (Figure 1), gives an extrapolated mean molecular area,  $A = 22.4 \pm 0.2 \text{ \AA}^2$ . This value may be compared to that for stearic acid, *ca.*  $18 \text{ \AA}^2/\text{molecule}$ . However, **I** contains two  $\text{C}_{18}$  chains per molecule, and simple molecular mechanics (MM2) calculations predict a limiting mean molecular area,  $A = 47 \text{ \AA}^2/\text{molecule}$ , for monolayer coverage. Since the packing of this molecule is expected to be limited by the alkyl chains, not the small carbon–sulfur ring, this observation suggests that the film on the trough is not a monolayer. The highly lipophilic species, **I**, is quite water-insoluble, mitigating against dissolution as an explanation for the anomalous limiting value of  $A$ . Low values of  $A$  can arise in the case of aggregated structures, such as micelles and vesicles. However, if this were the case, the ratio of limiting  $A$  to that expected for a monolayer would not be expected to have any particular value, whereas the observed ratio is very close to 2.0. Additionally, the transfer ratio was found to be variable in the range  $1.4 \leq \tau \leq 3.5$  and to depend strongly on the transfer conditions. For all of these reasons, the most likely explanation for the anomalous value of  $A$  is the formation of a bilayer of **I** at the air–water interface. In other respects, films of **I** at the air–water interface are relatively well-behaved. For example, the film is stable until  $\pi \geq 38 \text{ mN/m}$ .

Figure 1 inset shows the UV absorption spectrum of the film on  $\text{SiO}_2$ . The position and line shape of the 384 nm band are almost the same as those obtained for  $\text{CHCl}_3$  or dioxane solutions of **I**. X-ray crystallographic analysis of  $\text{C}_3\text{S}_5$  derivatives indicates that the ring adopts a  $\text{C}_{2v}$  symmetry.<sup>13</sup> The HMO calculation of the electronic structure of the  $\text{C}_3\text{S}_5$  ring gives eight energy levels:  $-14.27$ ,  $-12.71$ ,  $-11.03$ ,  $-10.00$ ,  $-9.86$ ,  $-9.4$ ,  $-8.06$ , and  $-7.92 \text{ eV}$ . Figure 2 is a pictorial description of the calculated HMO results. The allowed transitions (with oscillator strength  $f$  larger than 0) were found to be  $\pi_2 \rightarrow \pi_{-2}$  ( $f = 0.19$ ),  $\pi_2 \rightarrow \pi_{-3}$  ( $f = 0.12$ ), and  $\pi_2 \rightarrow \pi_{-5}$  ( $f = 0.02$ ). The former two transitions correspond to wavelengths at 435 and 375 nm, respectively. The symmetries of these transitions indicate that the transition dipole moments are along the  $\text{C}_2$  axis of the ring. Since these two transitions are close in energy and

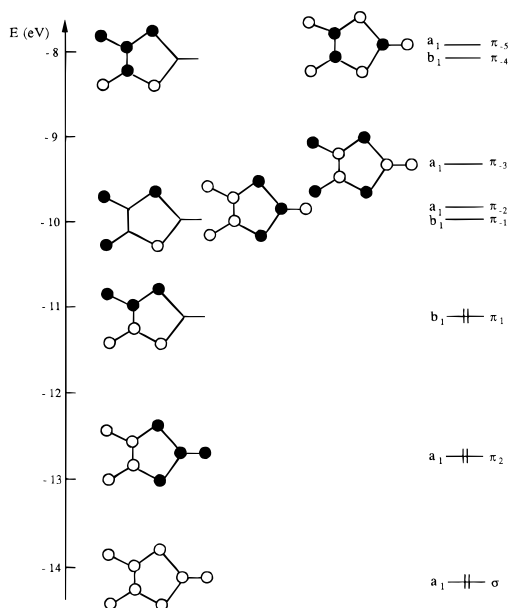


**Figure 2.** Calculated Hückel MO diagram for the  $C_3S_5$  ring.

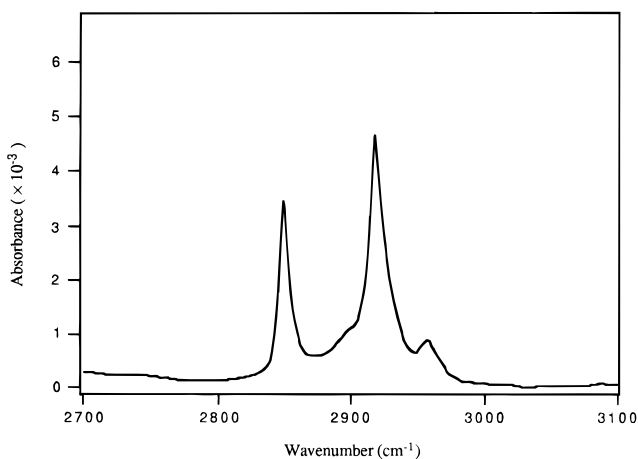


**Figure 3.** FTIR absorption spectrum in the C–H stretching region of the LB film of  $C_3S_5(C_{18}H_{37})_2$  on  $SiO_2$ .

have the same symmetry, they will interact with each other, resulting in the enhancement of one transition and the diminution of the other; however, the symmetry of the transition will be conserved. Unfortunately, the HMO calculation cannot take configuration interaction into account. PPP calculations with CI treatment predict that the principal absorption band occurs at 372 nm ( $f = 0.67$ ), which is in excellent agreement with the observed 384 nm band. Considering all these observations, it is clear that the allowed transition is oriented along the  $C_2$  axis of the  $C_3S_5$  subunit of **I**.

Further evidence for ordering comes from the transmission geometry infrared absorption spectrum in the C–H stretching region of a transferred film of **I** on fused quartz (Figure 3). The spectrum exhibits intense bands at 2849 and 2918  $cm^{-1}$ , assigned to symmetric,  $\nu_s$ , and asymmetric,  $\nu_{as}$ ,  $CH_2$  stretching vibrations, respectively. The position and the relatively low value of the full width at half-height (fwhh) of the  $\nu_{as}(CH_2)$  band, 13  $cm^{-1}$ , indicate that the film is well-ordered, due to the well-known correlation of band position and line width with gauche defect density.<sup>16</sup> In addition, the signal magnitudes in the IR spectra support the multilayer hypothesis. Although orientation of the C–H dynamic dipole relative to the electric vector polarization direction certainly has an effect on signal strength, in these experiments, it is clear that films of **I** exhibit signal strengths  $\geq 4$  larger than those observed in monolayer

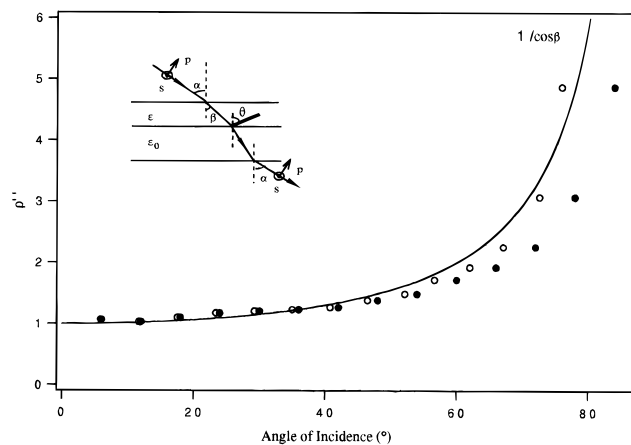


**Figure 4.** Change of  $\rho''$  as a function of the angle of incidence  $\alpha$  for the UV transition of  $C_3S_5(C_{18}H_{37})_2$  at 384 nm, ( $\bullet$ ), and after fitting to the  $\rho'' \sim \rho''(\beta)$  relationship ( $\circ$ ). The effective angle of incidence,  $\beta$ , is obtained from Snell's law with  $n_{eff} = 1.025$ . The solid line is the  $1/\cos\beta$  curve. The inset is a schematic of the transmission geometry in which LD experiments for uniaxially oriented samples are implemented. The excitation beam is incident at an angle  $\alpha$ , and  $\beta$  is the effective angle of incidence. Dielectric constants  $\epsilon$  and  $\epsilon_0$  refer to the LB film and  $SiO_2$ , respectively. The dipole has a population orientation distribution centered at  $\theta$ . All angles are relative to the surface normal.

samples, e.g., of stearic acid transferred to  $SiO_2$ . While, in the absence of detailed structure information, this comparison can only be qualitative, it does support the model in which multilayers of **I** are transferred during LB deposition.

**3.2. Linear Dichroism Measurements.** LD measurements have been widely employed to determine average orientations of chromophores using UV–vis absorption,<sup>17</sup> infrared absorption,<sup>18</sup> and fluorescence emission.<sup>19</sup> Most prevalently, absorption measurements are used to obtain the dichroic ratio,  $\rho$ . Knowledge of a chromophore's transition dipole moment with respect to the molecular geometry then allows the orientation of the chromophore to be determined with respect to the surface normal.

Here we discuss the relationship between the dichroic ratio,  $\rho$ , and the orientation,  $\theta$ , of a linear transition dipole in absorption spectroscopies. Because the transmission geometry is of interest, we assume that the substrate has no absorption and that  $\epsilon$  is real, which is true for the fused quartz substrates used in these experiments. We also assume that the interfaces between the film, the slide, and the air are perfectly smooth and that the film is uniaxial. The dichroic ratio,  $\rho$ , is defined as the ratio between the absorbances for transverse electric (TE) and transverse magnetic (TM) polarized radiation. It has been shown that  $\rho$  can be decomposed<sup>20,21</sup> according to

$$\rho'' = \frac{\int A_s d\nu}{\int A_n d\nu} = (\cos \alpha)^{-1} \quad (1)$$

$$\rho' = \frac{\int A_n d\nu}{\int A_p d\nu} = \frac{\cos \alpha}{(\cos^2 \alpha) + 2(\sin^2 \alpha)(\cot^2 \theta)} \quad (2)$$

$$\rho = \frac{\int A_s d\nu}{\int A_p d\nu} = \frac{1}{(\cos^2 \alpha) + 2(\sin^2 \alpha)(\cot^2 \theta)} = \rho' \rho'' \quad (3)$$

where  $\alpha$  is the angle of incidence and  $\theta$  is the ensemble average orientation of the transition dipole moment relative to the surface normal, as shown in the inset of Figure 4.  $\int A_n d\nu$  is the

integrated band absorbance when the film surface is perpendicular to the propagation direction of the excitation beam.<sup>22</sup>  $\int A_s d\nu$  and  $\int A_p d\nu$  are the integrated band absorbances when the surface is rotated to different angles relative to the beam direction for s- and p-polarized radiation, respectively.

From eq 1, it is clear that  $\rho''$  is independent of transmission dipole orientation and cannot alone be used to determine  $\theta$ . It is, however, commonly observed that experimental measurements of  $\rho''$  deviate from the simple  $1/\cos \alpha$  relation, especially at grazing angles of incidence.<sup>21</sup> To understand the origin of this discrepancy, we consider the local field induced by dipole-dipole interactions of neighboring molecules. Calculation of the true local field with quantitative accuracy is a daunting task, since it requires detailed structural knowledge, which is almost never known. However, its effect can be handled readily by introducing the *ansatz* of an effective incident angle,  $\beta$ , which can be fit from experimental data for  $\rho''$ , effectively modeling the phenomenon as a change in the angle between the propagation direction of the incident light and the dipole moment. The external angle of incidence,  $\alpha$ , is thus altered to the effective angle of incidence,  $\beta$ .

If the thickness of a film is larger than the wavelength of the incident light, the refractive index of the film and Snell's law can be used to obtain  $\beta$  directly. However, for films whose thickness is smaller than  $\lambda$ , Snell's law loses its physical interpretation in terms of the direction of propagation of wave fronts. To extend the analysis to monolayer films, we start by assuming a uniform film has an effective refractive index  $n_{\text{eff}}$ . By choosing different  $n_{\text{eff}}$  values, the  $\rho''$  data is fit to the  $1/\cos \beta$  curve through the simplified relation  $\sin \alpha = n_{\text{eff}} \sin \beta$ . Since the film thickness is less than  $\lambda$ , its refractive index,  $n_{\text{eff}}$ , is not that of the bulk material, but rather depends strongly on the detailed structure and packing in the film. This revised angle of incidence,  $\beta$ , is then substituted for  $\alpha$  in eq 2 to calculate  $\theta$ . In this approach it is assumed that  $n_{\text{eff}}$  remains the same for s- and p-polarized radiation. This analysis is analogous to the approach to effective LD measurements used, for example, by Yoneyama and co-workers.<sup>23</sup>

The geometry of  $C_3S_5(C_{18}H_{37})_2$  on fused quartz substrates can be determined by measuring the orientation centroids of the ring plane and the alkyl chains, which is achieved by LD measurements in the UV and IR, respectively. Figure 4 shows the  $\rho''$  ratio of the UV transition dipole at 384 nm at different incident angles. It is obvious that the experimental results do not follow the  $1/\cos \alpha$  curve. After fitting,  $n_{\text{eff}}$  is found to be 1.025. In Figure 5,  $\rho'$  is plotted for various values of  $\theta$  using  $\beta$  as the angle of incidence.  $\theta$  is found to be  $69 \pm 4^\circ$ . Since the direction of the UV transition dipole at 384 nm is along the  $C_2$  axis of the  $C_3S_5$  ring, we conclude that the  $C_2$  axis of the ring is at  $69 \pm 4^\circ$  relative to the surface normal.

A similar analysis was used to interpret the angle-dependent transmission infrared spectra of this LB film for s- and p-polarization.  $\rho''$  and  $\rho'$  were measured for both  $\nu_s(\text{CH}_2)$  and  $\nu_{\text{as}}(\text{CH}_2)$  vibrational bands. Again, the effective angle of incidence was obtained by fitting  $\rho''$  to  $1/\cos \beta$  using Snell's law. The effective refractive index of this film was found to be  $n_{\text{eff}} = 1.06$ . Note that, for different transitions in different spectral regions, the effective refractive indices would not necessarily be expected to be the same. In addition, the value of  $n_{\text{eff}}$  determined from infrared measurements is larger than that from UV measurements, consistent with qualitative expectations based on nuclear contributions to the polarizability in the infrared. The two vibrational bands were found to have identical  $\rho''$  values at all angles of incidence, indicating that the two transitions are affected similarly by local field effects. Again

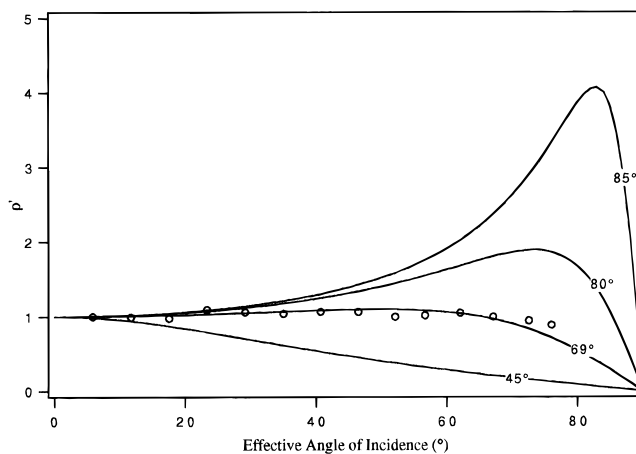


**Figure 5.**  $\rho'$  as a function of the effective angle of incidence  $\beta$  for the UV transition of  $C_3S_5(C_{18}H_{37})_2$  molecules at 384 nm. The solid lines are the calculated dependence of  $\rho'$  on the angle of incidence for different orientation angles.

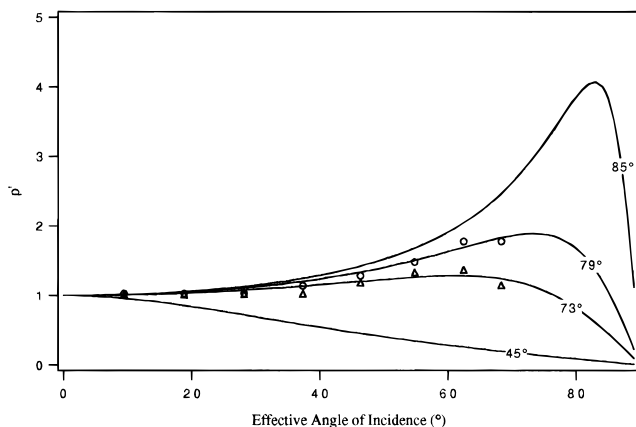


**Figure 6.**  $\rho'$  as a function of  $\beta$  for the symmetric ( $\Delta$ ) and asymmetric ( $\circ$ ) vibrational modes of  $\text{CH}_2$  groups of  $C_3S_5(C_{18}H_{37})_2$  molecules. The solid lines are the calculated dependence of  $\rho'$  on the angle of incidence for different orientation angles.

this is in qualitative agreement with expectations, since the transition dipoles for  $\nu_s(\text{CH}_2)$  and  $\nu_{\text{as}}(\text{CH}_2)$  are coplanar. By fitting the  $\rho'$  data to the calculated curves for different orientation angles, the orientation angles for symmetric and asymmetric vibrations of the  $\text{CH}_2$  group were found to be  $73 \pm 2^\circ$  and  $79 \pm 2^\circ$ , respectively, as shown in Figure 6.

The directions of the two  $\text{CH}_2$  vibrational modes and the chain axis are mutually orthogonal. This coupled with the highly ordered nature of the films, as deduced from the  $\nu_s(\text{CH}_2)$  and  $\nu_{\text{as}}(\text{CH}_2)$  band positions and line widths, means that their orientations relative to the surface normal are given by the following relation:<sup>24</sup>

$$\cos^2 \theta_{\text{chain}} + \cos^2 \theta_{\text{sym}} + \cos^2 \theta_{\text{asym}} = 1 \quad (4)$$

Thus, the long axes of the chains are found to orient at an angle of  $20 \pm 3^\circ$  relative to the surface normal. Information about the tilt of the  $C_{18}$  chains can be combined with the UV determination of the ring  $C_2$  axis orientation to eliminate a large number of possible molecular geometries. Although the data presented cannot unequivocally define the molecular geometry, both IR and UV-vis LD measurements are consistent with a packing in which the  $C_3S_5$  ring is nearly parallel to the surface and the  $C_{18}$  chains angle up sharply from the ring plane (vide infra).

**3.3. Angle-Resolved XPS Study of the Film Structure.** Remembering that the film of **I** at the air-water interface

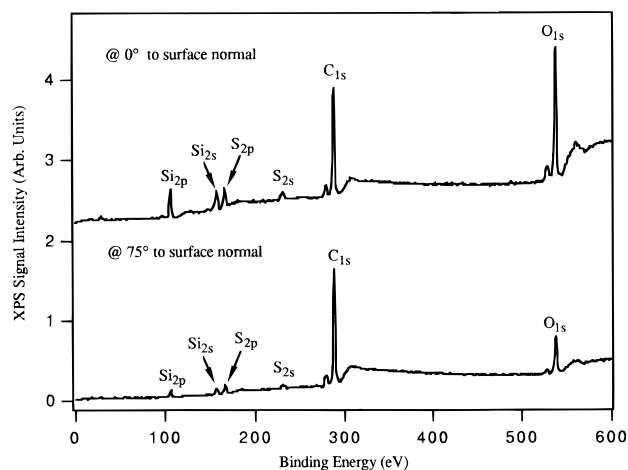


**Figure 7.** Angle resolved XPS survey spectra of  $C_3S_5(C_{18}H_{37})_2$  LB film on  $SiO_2$  substrate. Angles are referenced to the surface normal.

**TABLE 1: XPS Intensity Ratios**

	$I(C_{1s})/I(Si_{2p})$	$I(S_{2p})/I(Si_{2p})$
$0^\circ$	3.3	0.7
$75^\circ$	12.5	1.4

appeared to be a bilayer and that the transfer ratio of this film is variable, it is necessary to consider the possible structures which can account for a multibilayer film after transfer. Within the one-bilayer structure several configurations relative to the polar axis, i.e., surface normal, are possible: (a) head-to-head, (b) tail-to-tail, (c) head-to-tail, with tail on the top, and (d) tail-to-head, with head on the top, where head refers to the carbon-sulfur ring and tail to the alkyl chain. Angle-resolved XPS measurements were used to examine the relative ordering of those groups relative to the surface.

Figure 7 shows the XPS survey spectra of the LB film on a fused quartz slide at  $0^\circ$  and  $75^\circ$  collection angles relative to the surface normal. Due to fluctuations in the X-ray radiation source, changes in the sample position relative to the entrance window of the electron energy analyzer, and the angular distribution of the photoelectrons emitted from the surface, it was necessary to use an internal reference to normalize the photoelectron signal of each surface species. In this measurement, the  $Si_{2p}$  transition at 107 eV, arising from the  $SiO_2$  substrate, was used as the internal standard. The ratios between the total integrated band intensities of  $S_{2p}$  and  $Si_{2p}$  and that of  $C_{1s}$  were then used to assess the effect of changing the collection angle. Several features are immediately obvious from a qualitative inspection of the angle-resolved XPS spectra. First, both the  $O_{1s}$  and  $Si_{2p}$  signals are greatly diminished on going from  $0^\circ$  to  $75^\circ$  collection. Since molecule **I** contains neither Si nor O, these signals can come only from the substrate, and their diminution on going to grazing angle collection is consistent with the  $SiO_2$  substrate being located at a significant depth below the sample surface. In addition, the  $C_{1s}$  signal is enhanced relative to the other peaks on going to  $75^\circ$  collection, while the  $S_{2p}$  signal is diminished. Referring to Table 1, the  $I(S_{2p})/I(Si_{2p})$  ratio increases by a factor of ca. 2 on going from  $0^\circ$  to  $75^\circ$ , while the  $I(C_{1s})/I(Si_{2p})$  ratio increases by almost a factor of 4. These intensity ratios indicate that the S mass centroid lies above the substrate surface, but below that for the C centroid. In particular, they appear to rule out structures in which the carbon sulfide ring is topmost in the structure, i.e., the tail-to-tail and head on top structures enumerated above. For an isotropic layer a change in the collection angle only affects the probing depth, without affecting the detection probabilities for different surface

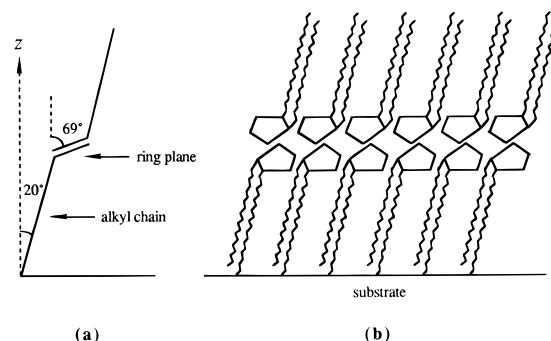


**Figure 8.** Proposed structure of the LB film of  $C_3S_5(C_{18}H_{37})_2$  molecules on  $SiO_2$ : (a) schematic diagram of the  $C_{18}$  alkyl tails and the  $C_3S_5$  ring plane relative to the surface normal; (b) possible stacking arrangement of  $C_3S_5(C_{18}H_{37})_2$  molecules consistent with spectroscopic data.

species. Thus, an increase in the ratio of  $I(C_{1s})/I(S_{2p})$  as the collection angle changes from  $0^\circ$  to  $75^\circ$  is consistent with the structure in which the long alkyl chains are on the top of the film with the  $C_3S_5$  rings laying underneath this alkyl layer.

Since XPS data indicate that the top layer of the film has a chain-up-ring-down structure, there are two possible models for the molecules in the second molecular layer of the film: (a) the chains are up and rings are down, or (b) the chains are down and rings are up. We propose that the second model is much more likely. The head-to-head structure allows for favorable  $\pi$ -stacking interactions among the head groups, which have been previously observed for related molecules in the solid state.<sup>5</sup> In addition, if the tail-to-head configuration were adopted, it is difficult to understand the propensity for bilayer formation as the structural motif at the air-water interface. On the other hand, a head-to-head configuration leads to bilayer formation in a natural way. The proposed structure of one bilayer is given in Figure 8, which depicts the known structural elements of these films and identifies the  $\pi$ -stacking interaction of the heterocycle head groups and van der Waals interactions among the  $C_{18}$  tails as the key interactions in driving the formation of the bilayer structure. The orientation of the  $C_3S_5$  ring plane is assumed to be the same as the orientation of the  $C_2$  axis of this heterocycle, though other possibilities cannot be ruled out. This structure model also permits the strong dependence of transfer ratio on deposition conditions to be understood. The head-to-head model given in Figure 8 would lead to relatively weak interactions among bilayer segments, thereby facilitating multibilayer formation during deposition. Such multibilayer formation is undoubtedly heterogeneous in the plane, giving rise to a macroscopically averaged transfer ratio which reflects that heterogeneity.

**3.4. The Local-Field Effect.** The role of the local-field effect has been studied in areas such as the coverage dependence of the adsorbate vibrational frequency,<sup>25</sup> surface-enhanced Raman spectroscopy,<sup>26</sup> differential reflectance spectroscopy,<sup>27</sup> and ellipsometry.<sup>28</sup> Here we provide a simple model to relate the local-field effect to fitted parameters from linear dichroism measurements and thus provide some physical interpretation of the effective angle,  $\beta$ . We assume that the molecules are identical and are confined to the first monolayer of a two-dimensional lattice. The lattice constant,  $a$ , is much smaller than the wavelength of incident light. We also assume that the film is uniform, and the surface coverage  $\Gamma = 1$ . A uniform applied external field  $\mathbf{E}_0$ ,  $\mathbf{E}_0 \equiv (\mathbf{E}_0 \cdot \hat{x} + \mathbf{E}_0 \cdot \hat{z})e^{i\omega_0 t}$ , which is the sum of the incident and reflected radiation, is present at the interface. The molecular electronic polarizability tensor  $[\alpha]$  of an adsorbed molecule is diagonal in the coordinate system of the substrate surface, with components  $\alpha_{||}$  and  $\alpha_{\perp}$ . The dipole

moment of the molecule induced by  $\mathbf{E}_0$  is

$$\mathbf{P} = \alpha_{\parallel} \mathbf{E}_s \quad \text{s-polarization} \quad (5a)$$

$$\mathbf{P} = \alpha_{\perp} \mathbf{E}_p \cos \xi + \alpha_{\parallel} \mathbf{E}_p \sin \xi \quad \text{p-polarization} \quad (5b)$$

where  $\xi$  is the angle of incidence. If the molecules are small compared to their average spacing, then they can be treated as point dipoles. A molecule at the  $\mathbf{r}_i$  site of the lattice will be affected by the local microscopic field  $\mathbf{E}_{\text{loc}}(\mathbf{r}_i)$ , which is the sum of the external field and the induced fields of other dipoles:

$$\mathbf{E}_{\text{loc}}(\mathbf{r}_i) = \mathbf{E}_0 + \left[ \sum_{j \neq i} -\nabla \frac{\mathbf{P}(\mathbf{r}_j)}{|\mathbf{r}_i - \mathbf{r}_j|^3} \right] \quad (6)$$

where  $\mathbf{P}(\mathbf{r}_j)$  is the dipole moment of the molecule at lattice site  $\mathbf{r}_j$  and is given by

$$\mathbf{P}(\mathbf{r}_j) = [\alpha] \mathbf{E}_{\text{loc}}(\mathbf{r}_j) \quad (7)$$

Since the substrate used is  $\text{SiO}_2$ , the substrate contribution to the local field is negligible.<sup>29</sup> After standard Fourier transform and lattice summing, taking the long-wavelength limit, the averaged microscopic local field is obtained.<sup>30</sup>

$$\mathbf{E}_{\text{loc},z} = \gamma_{\perp} \mathbf{E}_{0,z}, \quad \mathbf{E}_{\text{loc},x} = \gamma_{\parallel} \mathbf{E}_{0,x} \quad (8)$$

where the field correction factors are

$$\gamma_{\parallel} = \left[ 1 + \frac{A}{2a^3} \alpha_{\parallel} \right]^{-1} \quad (9a)$$

$$\gamma_{\perp} = \left[ 1 - \frac{A}{2a^3} \alpha_{\perp} \right]^{-1} \quad (9b)$$

where  $A$  is the two-dimensional lattice sum.

For a uniaxially anisotropic layer on an isotropic substrate, the spatial average of eq 6 and the continuity of molecular displacement give the two components of the effective high-frequency dielectric tensor of the film:<sup>31</sup>

$$\epsilon_{\parallel} = n_{\parallel}^2 = 1 + \frac{4\pi\alpha_{\parallel}\gamma_{\parallel}}{a^2d} \quad (10a)$$

$$\epsilon_{\perp} = n_{\perp}^2 = 1 + \frac{4\pi\alpha_{\perp}\gamma_{\perp}}{a^2d} \epsilon_2 \quad (10b)$$

where  $\epsilon_2$  is the dielectric constant of the substrate,  $n_{\parallel}$  and  $n_{\perp}$  are the parallel and perpendicular components of the effective refractive index of the film,  $d$  is the thickness of the film, and  $1/a^2d$  is molecular number density.

Now the expression for the effective refractive index of the thin film is correlated with the experimental data obtained from fitting of experimental values of  $\rho''$ . From eqs 9a and 10a one gets

$$\alpha_{\parallel} = \left[ \frac{4\pi}{a^2d(n_{\parallel}^2 - 1)} - \frac{A}{2a^3} \right]^{-1} \quad (11)$$

In order to use this analysis to characterize local field effects, it is first necessary to calculate the effective polarizabilities associated with each transition. In the analysis we assume that  $n_{\parallel} = n_{\text{eff}}$ , since  $n_{\text{eff}}$  is obtained from a normal incidence measurement in which the electric vector is entirely in-plane relative to the surface. For the electronic transition at 384 nm the pertinent part of the molecule is the  $\text{C}_3\text{S}_5$  ring. The lattice

constant is set from MM2 calculations to be  $a = 6.9 \text{ \AA}$ , and the thickness of the ring plane is determined from molecular modeling to be  $d \approx 2 \text{ \AA}$ . Thus, the experimentally measured  $n_{\text{eff}} = 1.025$  produces an effective polarizability of  $\alpha_{\parallel} = 0.38 \text{ \AA}^3$ . Using this value of  $\alpha_{\parallel}$  in eq 9a produces a local field which is perturbed from the incident value by a factor 1.005. This minor perturbation is entirely consistent with the fact that  $n_{\text{eff}}$  is so close to the refractive index of the superstrate. For the infrared C—H stretching transitions, the pertinent part of the molecule is comprised of two long  $\text{C}_{18}$  chains. From the literature for the octadecyl group,  $a = 4.2 \text{ \AA}$  and  $d = 19 \text{ \AA}$ . Since  $n_{\text{eff}} = 1.06$ , a polarizability of  $\alpha_{\parallel} = 2.8 \text{ \AA}^3$  is obtained. Again, using this value of  $\alpha_{\parallel}$  in eq 9a produces a local field which is perturbed from the incident value by a factor 1.205. This larger perturbation of the incident field at infrared frequencies is consistent with the inclusion of nuclear contributions to the polarizability, which become accessible at these frequencies.

#### IV. Conclusions

The structure of the LB film of  $\text{C}_3\text{S}_5(\text{C}_{18}\text{H}_{37})_2$  on fused quartz slides has been studied using XPS, transmission UV, and IR absorption spectroscopy, and a detailed structural model is proposed based on these data. The LB isotherm of  $\mathbf{I}$  indicates it forms a well-defined bilayer on the  $\text{H}_2\text{O}$  subphase. Transfer of the bilayers to  $\text{SiO}_2$  results in multilayer formation, where the number of layers transferred is a strong function of the transfer conditions. Angle-resolved XPS data show that the molecules in the top layer of the film have a structure with the alkyl chains on top and the carbon—sulfur heterocycles in the interior. HMO and PPP calculations of the electronic structure of the  $\text{C}_3\text{S}_5$  subunit indicate that the transition dipole for the transition at 384 nm is coincident with the  $\text{C}_2$  axis of this head group. In the transmission LD measurements, the local-field effect plays an important role in the measurement of the orientation of both electronic and vibrational dipoles. The effective refractive index of a chromophore in a thin solid film is obtainable by fitting s-polarized absorption data to Snell's law. The effective angle of incidence thus obtained is employed to calculate the orientation of the dipole, resulting in a more accurate calculation of orientation than would be obtained otherwise. The orientation of the ring plane and the alkyl chains relative to the surface normal have thus been measured to be ca.  $69^\circ$  and  $20^\circ$ , respectively. The proposed bilayer structure favors a head-to-head configuration, considering the  $\pi$ -stacking interactions among the  $\text{C}_3\text{S}_5$  groups. Potential applications of this multisulfur heterocycle compound as thin solid films in areas such as molecular electronics and corrosion inhibition of metal surfaces will be subjects of further investigation.

**Acknowledgment.** We acknowledge the financial support of the Department of Energy under Grant DEFG02-91ER45439. We also thank Dr. Rich Haasch for his help in the XPS measurements.

#### References and Notes

- (1) Roberts, G., Ed. *Langmuir-Blodgett Films*; Plenum Press: New York, 1990.
- (2) Ulman, A. *Ultrathin Organic Film*; Academic Press: Boston, 1991.
- (3) (a) Laibinis, P. E.; Whitesides, G. M.; Allara, D. L.; Tao, Y.-T.; Parikh, A. N.; Nuzzo, R. G. *J. Am. Chem. Soc.* **1991**, *113*, 7152. (b) Laibinis, P. E.; Whitesides, G. M. *J. Am. Chem. Soc.* **1992**, *114*, 9022. (c) Garrell, R. L.; Chadwick, J. E.; Severance, D. L.; McDonald, N. A.; Myles, D. C. *J. Am. Chem. Soc.* **1995**, *117*, 11563. (d) Tour, J. M.; Jones, L.; Pearson, D. L.; Lamba, J. J. S.; Burgin, T. P.; Whitesides, G. M.; Allara, D. L.; Parikh, A. N.; Arre, S. V. *J. Am. Chem. Soc.* **1995**, *117*, 9529.

- (4) Galloway, C. P.; Rauchfuss, T. B. In *The Chemistry of Inorganic Ring Systems*; Steudel, R., Ed.; Elsevier Science: Amsterdam, 1992; p 25.
- (5) For recent reviews on TTF chemistry, see: (a) Jørgensen, T.; Hansen, T. K.; Becher, J. *Chem. Soc. Rev.* **1994**, *23*, 41. (b) Bryce, M. R. *Chem. Soc. Rev.* **1991**, *20*, 355. (c) Schukat, G.; Richter, A. M.; Fanghändel, E. *Sulphur Rep.* **1987**, *7*, 155.
- (6) (a) Yang, X.; Rauchfuss, T. B.; Wilson, S. *J. Am. Chem. Soc.* **1989**, *111*, 3465. (b) Doxsee, D. D.; Galloway, C. P.; Rauchfuss, T. B.; Wilson, S. R.; Yang, X. *Inorg. Chem.* **1993**, *32*, 5467.
- (7) Sterimecke, G.; Sieler, H.; Dietzsch, W.; Hoyer, E. *Phosphorus Sulfur* **1982**, *12*, 237.
- (8) Olk, R.; Olk, B.; Dietzsch, W.; Kirmse, R.; Hoyer, E. *Coord. Chem. Rev.* **1992**, *117*, 99.
- (9) (a) Dourthe, C.; Izumi, M.; Garrigou-Lagrange, C.; Buffeteau, T.; Delhaes, P. *J. Phys. Chem.* **1992**, *96*, 2812. (b) Nakamura, T.; Tanaka, H.; Kojima, K.; Matsumoto, M.; Tachibana, H.; Tanaka, M.; Kawabata, Y. *Thin Solid Films* **1989**, *179*, 183. (c) Miura, Y. F.; Isotalo, H.; Kawaguchi, K.; Nakamura, T.; Matsumoto, M. *Appl. Phys. Lett.* **1993**, *63*, 1705. (d) Xiao, Y.; Yao, Z.; Jin, D. *J. Phys. Chem.* **1993**, *97*, 8519.
- (10) Streitwieser, A. *Molecular Orbital Theory*; John Wiley & Sons: New York, 1961.
- (11) (a) Murrell, J. H. *Theory of the Electronic Spectra of Organic Molecules*; Wiley and Sons: New York, 1963. (b) Pariser, R.; Parr, R. G. *J. Chem. Phys.* **1953**, *21*, 466. (c) Pople, J. A. *Trans. Faraday Soc.* **1953**, *21*, 466. (c) Pople, J. A. *Trans. Faraday Soc.* **1953**, *49*, 1375.
- (12) (a) Steimecke, G.; Kirmse, R.; Hoyer, E. *Z. Chem.* **1975**, *15*, 28. (b) Steimecke, G. Ph.D. Thesis, University of Leipzig, 1977. (c) Steimecke, G.; Sieler, H.; Kirmse, R.; Hoyer, E. *Phosphorus Sulfur* **1979**, *7*, 49.
- (13) Lindqvist, O.; Anderson, L.; Sieler, J.; Steimecke, G. Hoyer, E. *Acta Chem. Scand. A* **1982**, *36*, 855.
- (14) Mataga, N.; Nishimoto, K. *Z. Phys. Chem. (Frankfurt)* **1957**, *13*, 140.
- (15) (a) Fabian, J.; Mehlhorn, A.; Zahradnik, R. *J. Phys. Chem.* **1968**, *72*, 3975. (b) Gleiter, R.; Schmidt, E.; Johnson, P.; Cowan, D. O. *J. Am. Chem. Soc.* **1973**, *95*, 2680.
- (16) (a) Maoz, R.; Sagiv, J. *J. Colloid Sci.* **1984**, *100*, 65. (b) Porter, M. D.; Bright, T. B.; Allara, D. L.; Chidsey, C. E. D. *J. Am. Chem. Soc.* **1987**, *109*, 3559. (c) Byrd, H.; Pike, J. K.; Talham, D. R. *Thin Solid Films* **1994**, *242*, 100.
- (17) (a) Stayton, P. S.; Olinger, J. M.; Jiang, M.; Bohn, P. W.; Sligar, S. G. *J. Am. Chem. Soc.* **1992**, *114*, 9289. (b) Chou, H.; Chen, C.-T.; Stork, K. F.; Bohn, P. W.; Suslick, K. S. *J. Phys. Chem.* **1994**, *98*, 383.
- (18) (a) Hasegawa, T.; Umemura, J.; Takenaka, T. *J. Phys. Chem.* **1993**, *97*, 9009. (b) Spanget-Larsen, J.; Waluk, J.; Eriksson, S.; Thulstrup, E. *W. J. Am. Chem. Soc.* **1992**, *114*, 1942.
- (19) Albinsson, B.; Kubista, M.; Sandros, K.; Nordén, B. *J. Phys. Chem.* **1990**, *94*, 4006.
- (20) Cropek, D. M.; Bohn, P. W. *J. Phys. Chem.* **1990**, *94*, 6452.
- (21) Xu, Z.; Lau, S.; Bohn, P. W. *Surf. Sci.* **1993**, *296*, 57.
- (22) Ohta, N.; Matsunami, S.; Okazaki, S.; Yamazaki, I. *Langmuir* **1994**, *10*, 3909.
- (23) Yoneyama, M.; Sugi, M.; Saito, M.; Ikegami, K.; Kuroda, S.; Iizima, S. *Jpn. J. Appl. Phys.* **1986**, *25*, 961.
- (24) Ren, Y.; Meuse, C. W.; Hsu, S. L.; Stidham, H. D. *J. Phys. Chem.* **1994**, *98*, 8424.
- (25) Mahan, G. D.; Lucas, A. A. *J. Chem. Phys.* **1978**, *68*, 1344.
- (26) (a) King, F. W.; Van Duyne, R. P.; Schatz, G. C. *J. Chem. Phys.* **1978**, *69*, 4472. (b) Murray, C. A.; Bodoff, S. *Phys. Rev. Lett.* **1984**, *52*, 2273. (c) Eesley, G. L.; Smith, J. R. *Solid State Commun.* **1979**, *31*, 815.
- (27) Bagchi, A.; Barrera, R. G.; Dasgupta, B. B. *Phys. Rev. Lett.* **1980**, *44*, 1475.
- (28) Habraken, F. H. P. M.; Gijzman, O. L. J.; Bootsma, G. A. *Surf. Sci.* **1980**, *96*, 482.
- (29) Bootsma, G. A.; Meyer, F. *Surf. Sci.* **1969**, *14*, 343.
- (30) (a) Murray, C. A.; Bodoff, S. *Phys. Rev. B* **1985**, *32*, 671. (b) De Wette, F. W.; Schacher, G. E. *Phys. Rev.* **1965**, *137*, A78.
- (31) Quentel, G.; Kern, R. *Surf. Sci.* **1976**, *55*, 545.